

TRANSIENT HEATING OF COAL-WATER SLURRY DROPLETS

Phuoc X. Tran and Mahendra P. Mathur
Pittsburgh Energy Technology Center
Pittsburgh, PA. 15236

1. INTRODUCTION

Although many advantages can be derived from the use of CWF, the relatively large quantities of water in these fuels causes difficulties with ignition and flame stability. In addition, agglomeration of coal particles within the fuel droplets has been commonly observed to result in reduced combustion efficiency. Therefore, it is necessary to investigate the behavior of a CWF droplet undergoing heating and evaporation and the transient processes occurring in the interior of a CWF during this period so that processes such as disruptive burning, volatile release, combustion characteristics etc... are reliably predicted.

Theoretical model for the present analysis is illustrated in Fig. 1. For this droplet, the solid loading is initially large so that as the liquid component vaporizes, the evaporation front propagates into the interior of the droplet. In the wake of the evaporation front, coal particles support each other to form a porous shell keeping the droplet size constant during the evaporation history. The droplet now contains two different regions of consideration: the inner binary core whose surface is regressing with time and the porous shell which is thickening as the evaporation front moves. Thus the problem involves heating of the inner binary core, diffusion transport of the water vapor produced at the moving interface, and the diffusion transport of heat from an outer spherical boundary through the spherical porous shell of coal particle agglomerate. In addition to the complex phenomena, the inherent difficulties in the analysis are also due to the nonlinear nature of the moving interface and the transient behavior of the boundary conditions. Because of these difficulties any attempt to formulate any analytical solution must be accompanied with various model assumptions [1,2]. Such an attempt will obtain only relatively simple solutions in parametric forms and, therefore, many complicated phenomena associated with a slurry droplet during heating and evaporation will not be resolved. The main purpose of the present analysis is to develop numerical procedures to calculate the temperature distributions in both regions and the motion of the evaporation front under various conditions of heating rates, particle sizes.

2. FORMULATION OF THE PROBLEM

The present analysis is carried out under following assumptions: (i) spherical symmetry is valid, (ii) thermal properties are constant, (iii) internal mass transport is neglected, (iv) evaporation during the initial heat-up is neglected, (v) surface absorption of the radiative heat flux is assumed and (vi) the droplets behave like single phase with following properties:

$$\rho_d = (1-\phi) \rho_c + \phi \rho_w \quad ; \quad m_d = \sum_i m_i \quad (1)$$

$$c_{p,d} = \sum_i Y_i c_{p,i} ; Y_i = \frac{m_i}{m_d} \quad (2)$$

where i is for coal and water; ϕ is the liquid volume fraction and it relates to m_c and m_w as:

$$m_c = (1-\phi) \rho_c V_d ; m_w = \phi \rho_w V_d \quad (3)$$

and the droplet thermal conductivity is calculated using Lee and Taylor analysis [3] as:

$$\frac{\lambda_d}{\lambda_w} = \frac{2\phi + (2-\phi) \lambda_c/\lambda_w}{3 - \phi (1-\lambda_c/\lambda_w)} \quad (4)$$

We define the following dimensionless groups for the present analysis:

$$\theta_i = \frac{T_i - T_0}{T_b - T_0} ; U_i = r\theta_i ; i = d, c \quad (6)$$

$$\tau = \alpha_d t / r_s^2 ; \xi = r/r_b ; n = (r-r_b)/(r_s-r_b) \quad (7)$$

$$\sigma = r_b/r_s ; \beta = \alpha_c/\alpha_d ; \kappa = \lambda_c/\lambda_d \quad (8)$$

$$\gamma = \epsilon I_0 r_s / \lambda_d (T_b - T_0) + \lambda_g (\theta_g e^{-\theta_d, s}) / \lambda_d \quad (9)$$

$$v = \rho_d c_{p,d} (T_b - T_0) / \rho_w \phi \Delta H \quad (10)$$

The process of the droplet heating and evaporation are described as:

$$\text{At } 0 \leq \tau < \tau_p$$

$$\frac{\partial U_d}{\partial \tau} = \frac{\partial^2 U_d}{\partial \xi^2} \quad (11)$$

$$\text{At } \tau \geq \tau_p$$

for the binary core

$$\frac{\partial U_d}{\partial \tau} = \frac{1}{\sigma^2} \frac{\partial^2 U_d}{\partial \xi^2} + \frac{\xi}{\sigma} \frac{\partial U_d}{\partial \xi} \frac{d\sigma}{d\tau} \quad (12)$$

for the porous shell

$$\frac{\partial U_c}{\partial \tau} = \frac{\beta}{(1-\sigma)^2} \frac{\partial^2 U_c}{\partial n^2} - \left(\frac{n-1}{1-\sigma}\right) \frac{\partial U_c}{\partial n} \frac{d\sigma}{d\tau} \quad (13)$$

and the droplet surface regression rate is calculated by:

$$\frac{d\sigma}{d\tau} = \frac{v}{\sigma} \left[\frac{1}{r_b} \left(\frac{\partial U_d}{\partial \xi} \right)_{\xi=1} - \frac{c}{r_s - r_b} \left(\frac{\partial U_c}{\partial n} \right)_{n=0} + c - 1 \right] \quad (14)$$

These equations are subjected to the following conditions:

$$\text{At } \tau < 0 : U_d = 0 \quad (15)$$

$$\text{At } 0 \leq \tau < \tau_p : \sigma = 1 ; U_d(0) = 0 ; \left(\frac{\partial U_d}{\partial \xi} \right)_{\xi=1} = r_s (\gamma + \theta_{d,s}) \quad (16)$$

$$\text{At } \tau \geq \tau_p : U_d(0) = 0 ; U_c(0) = U_d(1) = r_b \quad (17a)$$

$$\left(\frac{\partial U_c}{\partial n} \right)_{n=1} = (r_s - r_b) \left(\frac{\gamma}{\kappa} + \theta_{c,s} \right) \quad (17b)$$

3. NUMERICAL CALCULATIONS

Numerical procedures developed by Tran and Mathur [4] are used. The spatial coordinate of Eqs. (11), (12) and (13) are discretized employing the usual central difference approximation. These discretized equations are used to transform these equations into a system of ordinary differential equations in temporal coordinates as:

At $0 \leq \tau < \tau_p$

$$\left(\frac{\partial U_d}{\partial \tau} \right)^i = \frac{U_d^{i+1} - 2U_d^i + U_d^{i-1}}{\Delta \xi^2} \quad (18)$$

At $\tau \geq \tau_p$

for the binary core:

$$\left(\frac{\partial U_d}{\partial \tau} \right)^i = \frac{U_d^{i+1} - 2U_d^i + U_d^{i-1}}{\sigma^2 \Delta \xi^2} + \frac{\xi}{\sigma} \left(\frac{U_d^{i+1} - U_d^{i-1}}{2\Delta \xi} \right) \frac{d\sigma}{d\tau} \quad (19)$$

for the porous shell:

$$\left(\frac{\partial U_C}{\partial \tau}\right)^i = \frac{\beta(U_C^{i+1} - 2U_C^i + U_C^{i-1})}{(1-\sigma)^2 \Delta \eta^2} - \left(\frac{n-1}{1-\sigma}\right) \left(\frac{U_C^{i+1} - U_C^{i-1}}{2\Delta \eta}\right) \frac{d\sigma}{d\tau} \quad (20)$$

where $i = 0$ to k , $k = 1/\Delta \xi$ for the binary core and $1/\Delta \eta$ for the porous shell.

The interface motion is now evaluated at $i = k$ for the binary core and $i = 0$ for the porous shell as:

$$\frac{d\sigma}{d\tau} = \frac{\nu}{\sigma} \left[\frac{U_d^{k+1} - U_d^{k-1}}{2r_b \Delta \xi} - \frac{\kappa(U_C^1 - U_C^{-1})}{2\Delta \xi (r_s - r_b)} \right] + \kappa - 1 \quad (21)$$

To calculate the interface motion represented by Eq. (21), values of U_d^{k+1} and U_C^{-1} must be determined. Using conditions at the interface given by Eq. (17a), one can get:

$$\left(\frac{\partial U_d}{\partial \tau}\right)^k = \left(\frac{\partial U_C}{\partial \tau}\right)^0 = r_s \frac{d\sigma}{d\tau} \quad (22)$$

introducing Eq. (22) into Eq. (19) for $i = k$ and into Eq. (20) for $i = 0$ to obtain U_d^{k+1} and U_C^{-1} as:

$$U_d^{k+1} = \frac{\left(r_s + \frac{U_d^{k-1}}{2\sigma \Delta \xi}\right) \frac{d\sigma}{d\tau} + \frac{2U_d^k - U_d^{k-1}}{\sigma^2 \Delta \xi^2}}{\frac{1}{\sigma^2 \Delta \xi^2} + \frac{\nu}{d\tau} / 2\sigma \Delta \xi} \quad (23)$$

$$U_C^{-1} = \frac{\left(r_s - \frac{U_C^1}{2(1-\sigma)\Delta \eta}\right) \frac{d\sigma}{d\tau} - \frac{\beta(U_C^1 - 2U_C^0)}{(1-\sigma)^2 \Delta \eta^2}}{\frac{\beta}{(1-\sigma)^2 \Delta \eta^2} - \frac{1}{2(1-\sigma)\Delta \eta} \frac{d\sigma}{d\tau}} \quad (24)$$

Hence value of $d\sigma/d\tau$ can be determined implicitly from Eqs. (21), (23) and (24) using method of halving of the interval. Using varying dimensionless time interval, and $\Delta \xi = \Delta \eta = 0.2$ these above equations are integrated using Adams-Moulton integration subroutine.

4. RESULTS AND DISCUSSION

The calculation was made for CWF droplet with 70 percent coal loading by weight heating and evaporation in an environment with $\lambda_g = 2.6 \times 10^{-4}$

cal/cm-s-K. Additional data for water are: $\rho_w = 1.0 \text{ g/cm}^3$; $c_{p,w} = 1.0 \text{ cal/g-K}$; $\lambda_w = 0.00146 \text{ cal/cm-s-K}$; $\Delta H = 540 \text{ cal/g}$ and $T_D = 373 \text{ K}$. For coal: $\rho_c = 1.3 \text{ g/cm}^3$; $c_{p,c} = 0.35 \text{ cal/g-K}$ and $\lambda_c = 0.0003 \text{ cal/cm-s-K}$.

Shown in Fig. 2 are the typical temperature profiles in the interior of the CWF droplet i.e. the profiles of both the inner binary sphere and the porous coal agglomerate shell for $I_0 = 400 \text{ W/cm}^2$, $r_s = 25 \text{ }\mu\text{m}$, $v = 1.326$. In this figure the intersection of the temperature profiles and $\theta_d = \theta_c = 1$ gives the location of the evaporation front while the thickness of the developed porous shell is given by the width between these locations and $\sigma = 1$. For this CWF droplet, the temperature profile that exists when the droplet surface temperature increases to the boiling temperature of the water is far from uniform. As the surface temperature reaches the boiling temperature of the water, two regions of temperature distributions within the CWF droplet ensue: the inner binary core, whose surface is regressing with time and the porous shell which is thickening as the evaporation front moves.

The effects of radiation heat flux, I_0 , droplet size, r_s , on the dimensionless temperature profiles of the binary core and of the porous shell are illustrated in Figs. 3a and 4a. To increase I_0 and r_s leads to an increase in the heating rate, the surface temperature will rise rapidly and the droplet temperature deep inside will lag further behind the surface temperature. Eventually large temperature gradient is established and the intra-droplet temperature does not have enough time to keep pace with the motion of the evaporation front which depends strongly on the internal temperature gradient as describe by Eq. (14). As a result, the inner binary core is heated essentially by the thermal wave moving with the evaporation front. To decrease I_0 and r_s results in lowering the heating rate, the surface temperature rises slowly and the internal temperature has enough time to keep pace with the surface temperature. In this instance, the internal temperature gradient is less significant leading to slow motion of the evaporation front. As a result, the heating of the binary core is due to thermal diffusion from the outer boundary.

The dimensionless temperature profiles of the porous shell of the coal particles agglomerate for various values of I_0 and r_s were also illustrated in Figs. 3b and 4b. As shown, the temperature of the porous shell is distributed linearly across the porous shell for values of I_0 and r_s used in the present analysis. Under opposite condition, such a linear distribution, however, was found only in the region closed to the droplet surface. As shown, the surface temperature is substantially higher than the boiling temperature of the liquid component and is also higher at higher radiant heat flux, I_0 , large particle size, r_s .

5. CONCLUSION

A simple analysis has been made to investigate the transient processes occurring in the interior of a CWF droplet undergoing heating and evaporation. Two heating mechanisms have been obtained: at low heating rate the rate of heat diffusion is faster than the rate of the evaporation front motion, the transient heating of the inner binary core is controlled by diffusion and vanishes quickly after the evaporation begins. However, under opposite conditions, the rate of the motion of the evaporation is faster than the rate of the energy diffusion, the transient heating of the inner binary core occupies the entire period of evaporation and is controlled by the thermal wave moving with the evaporation front. The present numerical

technique is powerful for this kind of moving boundary and phase change problem.

NOMENCLATURE

c_p	-	specific heat
ΔH	-	heat of evaporation
I_o	-	radiant heat flux
r	-	r-coordinate
r_b	-	evaporation front location
r_s	-	droplet radius
T	-	temperature
T_b	-	temperature
T_o	-	initial particle temperature
t	-	time

Greek Symbols

α	-	thermal diffusivity
ϵ	-	emissivity
λ	-	thermal conductivity
ρ	-	density

Subscripts

b	-	evaporation front location
c	-	coal
d	-	droplet
e	-	ambient condition
g	-	gas phase
p	-	pyrolysis
s	-	surface
w	-	water

REFERENCES

1. P. Antaki, Transient Processes in a Rigid Slurry Droplet During Liquid Vaporization and Combustion, Combustion Science and Technology, 46, 113-135, (1986).
2. G. F. Carey and P. Murray, Perturbation Analysis of The Shrinking Core, Chem. Eng. Sci., 44, 979-983, (1989).
3. T. Y. R. Lee and R. E. Taylor, Thermal Diffusivity of Dispersed Material, J. of Heat Transfer, 400, 720-724, (1978).
4. P. X. Tran and M. P. Mathur, "Transient Heating of Coal Particles Undergoing Pyrolysis," 23rd Symposium (International) on Combustion, in press.

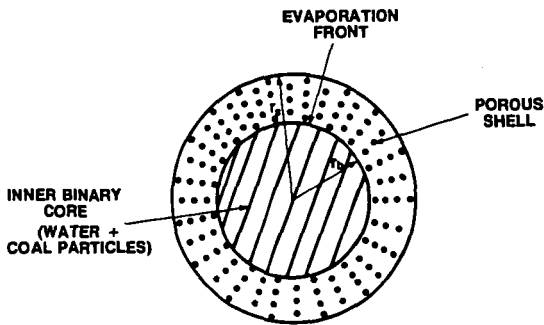


Figure 1. Theoretical Model.

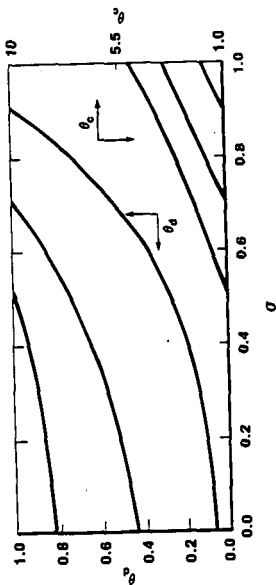


Figure 2. Temperature Profiles of a CHF droplet Undergoing Heating and Evaporation; ($T_0 = 400 \text{ K/cm}^2$; $r_0 = 25 \text{ \mu m}$; $\nu = 1.326$).

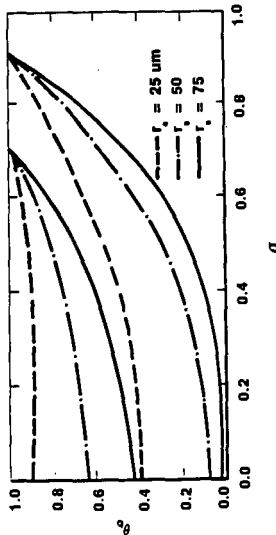


Figure 3a. Effect of Droplet Size, r_0 , on the Temperature Profiles of the Inner Binary Core; ($T_0 = 400 \text{ K/cm}^2$; $\nu = 0.246$).

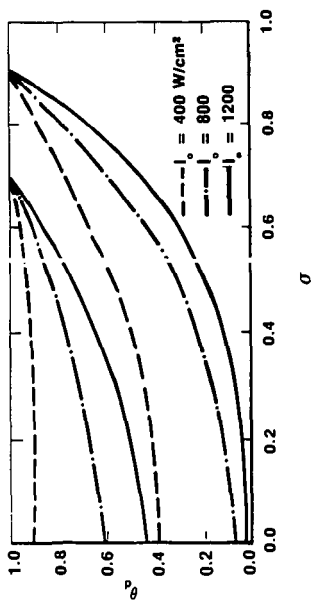


Figure 4a. Effect of Heat Flux, I_0 , on the Temperature Profiles of the Inner Binary Core; ($r_s = 25 \mu\text{m}$, $v = 0.246$).

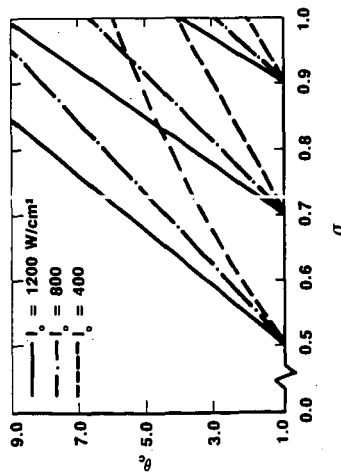


Figure 4b. Effect of Heat Flux, I_0 , on the Temperature Profiles of the Porous Shell; ($r_s = 25 \mu\text{m}$, $v = 0.246$).

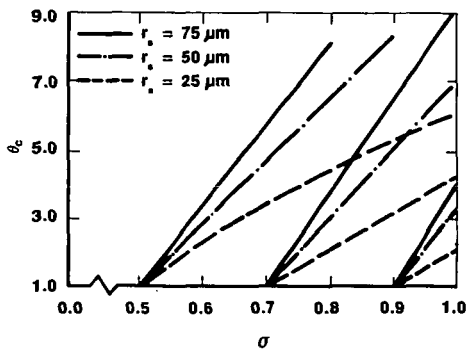


Figure 3b. Effect of Droplet Size, r_s , on the Temperature Profiles of the Porous Shell; ($I_0 = 400 \text{ W/cm}^2$; $v = 0.246$).